Dynamic Analysis of Rectilinear Motion of a Self-Propelling Disk With Unbalance Masses

T. Das
Graduate Student

R. Mukherjee
Associate Professor
Assoc. Mem. ASME

Department of Mechanical Engineering,
Michigan State University,
2555 Engineering Building,
East Lansing, MI 48824-1226

This paper investigates the dynamics of a rolling disk with three unbalance masses that can slide along radial spokes equispaced in angular orientation. The objective is to design trajectories for the masses that satisfy physical constraints and enable the disk to accelerate or move with constant velocity. The disk is designed to remain vertically upright and is constrained to move along a straight line. We design trajectories for constant acceleration, first using a static model, and then through detailed analysis using a dynamic model. The analysis based on the dynamic model considers two separate cases; one where the potential energy of the system is conserved, and the other where it continually varies. Whereas trajectories conserving potential energy are quite similar to those obtained from the static model, the variable potential energy trajectories are the most general. A number of observations related to the system center-of-mass are made with respect to both trajectories. Following the strategy for constant acceleration maneuvers, we give a simple approach to tracking an acceleration profile and provide some simulation results. [DOI: 10.1115/1.1344903]

1 Introduction

Ever since its invention, the wheel has been used primarily as a quasi-static device. Enhanced mobility and stability have been achieved using multiple wheels, large wheels, broad wheel bases, multiwheel drives, etc. Only in the recent past, researchers proposed wheels that are dynamical entities. The Gyrover proposed by Brown and Xu [1], for example, is a dynamically stabilized single-wheel robot that uses gyroscopic forces for steering and stability. The Gyrover, in which the wheel and the vehicle are one and the same, has a number of advantages over multiwheeled vehicles. Before the introduction of Gyrover, a few designs were proposed for spherical wheels with internal propulsion mechanisms. An omnidirectional robot comprised of a spherical wheel, an arch-shaped body, and an arm-like mechanism, was proposed by Koshiyama and Yamafuji [2]. In two different designs proposed by Halme et al. [3] and Bicchi et al. [4], a device constrained to roll inside the spherical cavity creates unbalance and generates motion. A change in heading is produced by turning the wheel axis. Both designs complicate the control problem by imposing nonholonomic constraints, internal and external to the spherical shell.

To simplify the control problem and from practical considerations, we proposed a spherical robot design ([5]), where the propulsion mechanism is fixed to the outer skeleton. The propulsion mechanism is comprised of four unbalance masses that are controlled along radial spokes; the extremities of the spokes define the vertices of a regular tetrahedron. The control of the four masses to achieve a desired motion of the spherical wheel poses a complicated and challenging problem in dynamics and control. To get insight into this problem, we study the planar case in this paper. We investigate the dynamics of a rolling disk with three unbalance masses, constrained to slide along radial spokes, configured 120 deg apart from one another. For this system, shown in Fig. 1, we propose to control the motion of the masses such that the disk center can have a specified constant acceleration. We also investigate optimal transition of the disk acceleration from one value to another. These problems are relevant since a trajectory of the disk can be specified in terms of an acceleration profile.

Besides the mechanism comprised of reciprocating masses, shown in Fig. 1, a number of other mechanisms can be designed for propelling the disk. For example, a heavy mass constrained to roll on the inner perimeter can create mass eccentricity and cause the disk to roll. Planar versions of the designs by Halme et al. [3] and Bicchi et al. [4] conform to this category. Also, a spinning rotor mounted on the disk can generate reaction torque and cause the disk to roll. This mechanism, with an additional rotor that allows control of the disk inclination, has been extensively studied by Ehlers et al. [6] and Yavin [7,8]. In their studies the complete dynamics of the disk and rotors were considered, and the nonlinear control problems of tracking and point-to-point stabilization were addressed. A number of other authors (Getz [9] and Rui and McClamroch [10], for example) have also addressed the stabilization problem in the rolling disk but few have investigated the dynamics of viable propulsion mechanisms.

In this paper, we first describe a propulsion mechanism for a vertically upright rolling disk, constrained to move along a straight line. In Section 3 we present preliminary analysis of the mechanism based on a static model. Two solutions are presented in this section for uniform acceleration of the disk along a straight line. The first solution identifies via-points and interpolates sinusoids to generate approximately constant acceleration trajectories. The trajectories conserve potential energy and suggest further analysis on the basis of potential energy. The second solution is optimal in the sense that it minimizes a component of the kinetic energy. It also renders the moment of inertia of the disk invariant with orientation and provides greater freedom in trajectory design. A dynamic model of the system is developed in Section 4 and uniform acceleration maneuvers that conserve potential energy are once again investigated. The variable potential energy trajectories are studied in Section 5. Similar to the static model, the trajectories conserving potential energy are limacons, and identical for the unbalance masses. The variable potential energy trajectories, which are not limacons, are described by five constants of motion and present the most general solution. In Section 6 we present an optimal approach to tracking an acceleration profile along with simulation results. Section 7 provides concluding remarks.

Contributed by the Applied Mechanics Division of THE AMERICAN SOCIETY OF MECHANICAL ENGINEERS for publication in the ASME JOURNAL OF APPLIED MECHANICS. Manuscript received by the ASME Applied Mechanics Division, June 24, 1999; final revision, April 16, 2000. Associate Editor: N. C. Perkins. Discussion on the paper should be addressed to the Editor, Professor Lewis T. Wheeler, Department of Mechanical Engineering, University of Houston, Houston, TX 77204-4792, and will be accepted until four months after final publication of the paper itself in the ASME JOURNAL OF APPLIED MECHANICS.

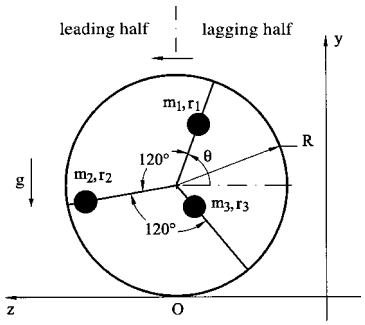

Fig. 1 The disk with reciprocating masses

2 Description of Propulsion Mechanism

A schematic description of the self-propelled disk is shown in Fig. 1. The radial lines from center of the disk to the circumference represent spokes, each of which carries a lumped mass. The masses, denoted by m_1, m_2, m_3, are of equal magnitude, m, and slide along their respective spokes. The angular position of mass m_1 is measured counter clockwise from the negative z-axis, and is denoted by θ. The masses m_2, m_3, are located 120 deg and 240 deg apart with respect to m_1. The radial positions of the masses are denoted by r_1, r_2, and r_3, respectively. For ease of explanation, we divide the disk area into two distinct halves: the ''leading half'' and the ''lagging half.'' The gravitational force of a mass in the leading half contributes positive moment and causes the disk to accelerate; the gravitational force of a mass in the lagging half causes the disk to deccelerate. Now consider a static model of the mechanism, which ignores the inertia forces of the unbalance masses. For this model, which is valid for small velocities and accelerations, we have

$$I(\theta)\ddot{\theta} = -mg[r_1 \cos\theta + r_2 \cos(\theta + 120°) + r_3 \cos(\theta - 120°)] \quad (1)$$

where, $I(\theta)$ is the mass moment of inertia of the entire assembly about the instantaneous center of rotation, O, which can be expressed as

$$I(\theta) \triangleq I_{ds} + 3mR^2 + m(r_1^2 + r_2^2 + r_3^2) + 2mR[r_1 \sin\theta + r_2 \sin(\theta + 120°) + r_3 \sin(\theta - 120°)]. \quad (2)$$

It is implicitly assumed in Eq. (1) that the friction force between the disk and the ground prevents the disk from slipping. In Eq. (2), I_{ds} represents the combined moment of inertia of the disk and spokes about O. The unbalance masses are constrained by the relation $0 \leqslant r_1, r_2, r_3 \leqslant R$, where R is the length of each spoke.

We designed our mechanism with three masses since fewer masses cannot maintain constant acceleration. For a single mass, this is evident from the equation of motion

$$r_1 = -\frac{I_1(\theta)\ddot{\theta}}{mg\cos\theta}, \quad I_1(\theta) \triangleq I_{ds} + m(R^2 + r_1^2 + 2r_1 R \sin\theta)$$

which indicates that constant $\ddot{\theta}$ cannot be achieved with r_1 satisfying $0 \leqslant r_1 \leqslant R$. For two masses, on spokes that are separated by an angle α, the equation of motion has the form

$$I_2(\theta)\ddot{\theta} = -mg[r_1 \cos\theta + r_2 \cos(\theta + \alpha)]$$

$$I_2(\theta) \triangleq I_{ds} + 2mR^2 + m(r_1^2 + r_2^2) + 2mR[r_1 \sin\theta + r_2 \sin(\theta + \alpha)].$$

On simplification, we have

$$r_{eq} = -\frac{I_2(\theta)\ddot{\theta}}{mg\cos(\theta + \psi)} \quad r_{eq} \triangleq \sqrt{r_1^2 + r_2^2 + 2r_1 r_2 \cos\alpha},$$

$$\psi \triangleq \arctan\left(\frac{r_2 \sin\alpha}{r_1 + r_2 \cos\alpha}\right)$$

where $0 \leqslant \psi \leqslant \alpha$. Since $(\theta + \psi)$ will assume all angular positions during motion, r_{eq} cannot remain bounded for a constant acceleration. Therefore, two masses will not suffice. In the next three sections, we will show that three masses equispaced in angular orientation, as shown in Fig. 1, is capable of maintaining constant acceleration.

3 Preliminary Analysis Using Static Model

3.1 An Approximate Solution. In this section we present an approximate solution to the constant acceleration maneuver problem. We use the static model in Eq. (1) but assume the moment of inertia of the system to be constant. We divide the leading half into three phases, shown in Fig. 2. The presence of a mass in phase 1 necessitates the second mass to be present in phase 3 and the third mass in the lagging half. The presence of a mass in phase 2 necessitates the other two masses to be confined to the lagging half. Now consider the configuration in Fig. 3 where mass m_1 is on the boundary between phase 1 and phase 2. We use this configuration to determine the maximum acceleration of the disk that can be maintained for all values of θ. To achieve maximum acceleration in this configuration, we must have $r_1 = R$ and $r_3 = 0$. The instantaneous value of r_2 is not important since m_2 does not have a moment arm. The maximum acceleration in this configuration can be obtained from Eq. (1), as follows:

$$I\ddot{\theta} = -mgR\cos 150°.$$

To maintain this acceleration for all values of θ, the mass positions should satisfy

$$R\cos 150° = r_1 \cos\theta + r_2 \cos(\theta + 120°) + r_3 \cos(\theta - 120°).$$

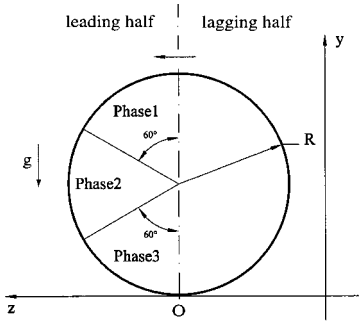

Fig. 2 Different phases in the leading half of the disk

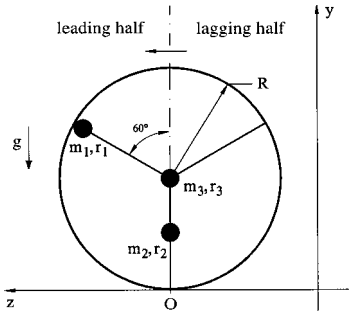

Fig. 3 A particular configuration of the reciprocating masses

In the neighborhood of $\theta=150°$, we have $r_3\approx 0$ and $r_1\approx R$. Hence, r_2 can be obtained as

$$r_2(150°)=\lim_{\theta\to 150°} R\frac{(\cos 150°-\cos\theta)}{\cos(\theta+120°)}=\frac{R}{2}.$$

A similar analysis can be carried out at $\theta=210°$ where m_1 is between phase 2 and phase 3. At this configuration, where $r_1=R$, and $r_2=0$, we can show that r_3 satisfies $r_3=R/2$.

Since the spokes are symmetrically located, we assume the mass trajectories to be identical with 120 deg phase shift from one another. The above analysis then implies that there are six via-points on the trajectory, namely

$$r_1=\begin{cases}0 & \text{for } \theta=30°,-30°\\ R/2 & \text{for } \theta=90°,270°\\ R & \text{for } \theta=150°,210°\end{cases}$$

By fitting sinusoids between these via-points, the approximate solution is obtained as

$$r_1(\theta)=\begin{cases}0 & \text{for } -30°\leqslant\theta\leqslant 30°\\ R[1-\cos(\theta-30°)] & \text{for } 30°\leqslant\theta\leqslant 90°\\ -R\cos(\theta+30°) & \text{for } 90°\leqslant\theta\leqslant 150°\\ R & \text{for } 150°\leqslant\theta\leqslant 210°\\ -R\cos(\theta-30°) & \text{for } 210°\leqslant\theta\leqslant 270°\\ R[1-\cos(\theta+30°)] & \text{for } 270°\leqslant\theta\leqslant 330°.\end{cases} \tag{3}$$

The trajectories of r_2 and r_3 can be simply obtained as

$$r_2(\theta)=r_1(\theta+120°),\quad r_3(\theta)=r_1(\theta-120°). \tag{4}$$

For example, $r_2(\theta)$ can be expressed as

$$r_2(\theta)=\begin{cases}0 & \text{for } 210°\leqslant\theta\leqslant 270°\\ R(1+\sin\theta) & \text{for } 270°\leqslant\theta\leqslant 330°\\ -R\cos(\theta+150°) & \text{for } -30°\leqslant\theta\leqslant 30°\\ R & \text{for } 30°\leqslant\theta\leqslant 90°\\ R\sin\theta & \text{for } 90°\leqslant\theta\leqslant 150°\\ R[1-\cos(\theta+150°)] & \text{for } 150°\leqslant\theta\leqslant 210°.\end{cases}$$

The following observations can now be made for the approximate solution. The trajectories of the masses are piecewise smooth with first derivative continuity. Also, they satisfy

$$r_1\sin\theta+r_2\sin(\theta+120°)+r_3\sin(\theta-120°)=0 \tag{5}$$

which implies conservation of potential energy. The moment of inertia of the system is, however, not constant. From Eq. (2), it can be expressed as

$$I_a=I_{ds}+3mR^2+m(r_1^2+r_2^2+r_3^2).$$

From the above equation it can be shown that I_a is comprised of a constant term and a periodic term. Therefore, the angular acceleration of the disk

$$\ddot{\theta}=-\frac{mgR\cos 150°}{I_a}\approx 0.866\frac{mgR}{I_a} \tag{6}$$

is not constant, but varies periodically. To complete the analysis, we note that a lower magnitude of acceleration can be generated by scaling down the trajectories of r_1, r_2, and r_3. This can be done by replacing R in Eq. (3) with R^*, $0\leqslant R^*\leqslant R$.

3.2 An Optimal Solution. In this section, we seek an optimal solution; one optimal in some sense of energy consumption. We impose the constraint that the potential energy is conserved and therefore Eq. (5) holds. This condition, which was satisfied by the approximate solution, is convenient and reduces the number of variable terms in the moment of inertia expression in Eq. (2).

By differentiating Eq. (5) with respect to θ and substituting Eq. (1), we obtain

$$r_1'\sin\theta+r_2'\sin(\theta+120°)+r_3'\sin(\theta-120°)=K,\quad K\triangleq\frac{I\ddot{\theta}}{mg} \tag{7}$$

where r_1', r_2', and r_3', are the derivatives of r_1, r_2, and r_3, respectively, with respect to θ, I represents the moment of inertia of the system given by Eq. (2), and $\ddot{\theta}$ denotes the specified constant acceleration of the disk. We now make the assumption that I is constant. In the ensuing analysis, we will show that I can be maintained at a constant value. By differentiating Eq. (1) with respect to θ and substituting Eq. (5), we get

$$r_1'\cos\theta+r_2'\cos(\theta+120°)+r_3'\cos(\theta-120°)=0. \tag{8}$$

Using Eqs. (7) and (8), we can express r_2' and r_3' in terms of r_1' as follows:

$$r_2'=r_1'-\frac{2}{\sqrt{3}}K\cos(\theta-120°)$$
$$r_3'=r_1'+\frac{2}{\sqrt{3}}K\cos(\theta+120°) \tag{9}$$

where K was defined in Eq. (7). With the objective of designing the optimal trajectory, we now define the cost functional

$$J=\int_0^{2\pi}L\,d\theta,\quad L\triangleq\frac{1}{2}m(r_1'^2+r_2'^2+r_3'^2) \tag{10}$$

where the integrand represents the pseudo-kinetic energy, or the kinetic energy that accounts for the motion of the masses in the reference frame of the spokes. With respect to an inertial frame, the masses will undergo both translation and rotation that will depend on the instantaneous angular velocity of the disk. During constant acceleration maneuvers, the angular velocity of the disk will increase linearly with time and the true kinetic energy will be a function of time. To investigate optimal trajectories that are functions of θ, rather than both θ and time, we choose the cost functional as the integral of the pseudo-kinetic energy.

To proceed with the optimization, we substitute the expressions for r_2' and r_3' into Eq. (9) to rewrite the integrand in Eq. (10) as follows:

$$L=\frac{1}{2}m\left(3r_1'^2+\frac{4}{3}K^2[\cos^2(\theta-120°)+\cos^2(\theta+120°)]-4Kr_1'\sin\theta\right).$$

Using the Euler-Lagrange equation ([11]) from calculus of variations

$$\frac{d}{d\theta}\left(\frac{\partial L}{\partial r_1'}\right)-\frac{\partial L}{\partial r_1}=0$$

for the stationary value of J, we obtain the trajectory of r_1 as follows:

$$r_1=C_1\theta-\frac{2}{3}K\cos\theta+C_2$$

where C_1 and C_2 are constants of integration. Since r_1 has to satisfy $0\leqslant r_1\leqslant R$, C_1 must be zero, and C_2 and K must lie in the shaded region of Fig. 4. The optimal trajectory will therefore be a limacon, of the form

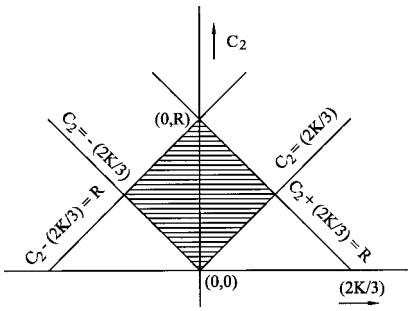

Fig. 4 Shaded region indicates feasible parameter values for the solution in Section 3.2

$$r_1 = C_2 - \frac{2}{3}K\cos\theta. \tag{11}$$

The optimal trajectories of r_2, r_3, can be derived using Eq. (4). The moment of inertia, which was assumed constant, can now be shown to be constant. From Eq. (2) we can show that

$$I_o = I_{ds} + m\left(3R^2 + 3{C_2}^2 + \frac{2}{3}K^2\right).$$

The constant acceleration of the disk can therefore be expressed as

$$\ddot{\theta} = \frac{mgK}{I_o}$$

where $-0.75R \leqslant K \leqslant 0.75R$, limits the maximum value of acceleration to $\ddot{\theta} = 0.75mgR/I_o$. The feasible range of values of K can be verified from Fig. 4.

Unlike the approximate solution, the optimal solution results in constant acceleration of the disk. The optimal solution is also smooth whereas the approximate solution is piecewise smooth with first derivative continuity. A single parameter R^* describes the family of approximate solutions. The particular solution where $R^* = R$ is shown in Eq. (3). Two parameters, C_2 and K, describe the family of optimal solutions. Clearly, the optimal solution provides greater freedom in trajectory selection. Despite differences, the trajectories for the approximate solution and the optimal solution, shown in Fig. 5, are strikingly similar.

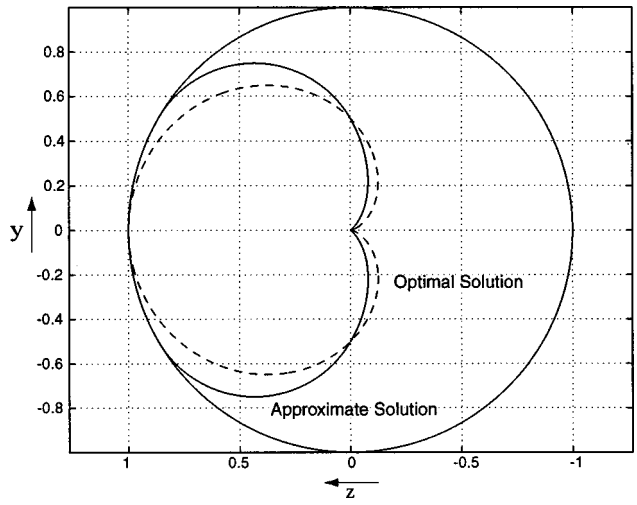

Fig. 5 Comparison of the approximate and optimal solutions for a disk of unity radius

4 Dynamic Model: Constant Potential Energy Maneuvers

4.1 Lagrangian Formulation. In this section we perform a detailed analysis of the problem using a dynamic model. To obtain Lagrange's equations, we first express the kinetic energy of the system as

$$T = \frac{1}{2}I_{ds}\dot{\theta}^2 + \frac{1}{2}m(v_1^2 + v_2^2 + v_3^2)$$

where v_1, v_2, and v_3, are the velocities of masses m_1, m_2, and m_3, respectively, and given by the relations

$$v_1^2 = R^2\dot{\theta}^2 + \dot{r}_1^2 + {r_1}^2\dot{\theta}^2 - 2R\dot{\theta}\dot{r}_1\cos\theta + 2Rr_1\dot{\theta}^2\sin\theta$$

$$v_2^2 = R^2\dot{\theta}^2 + \dot{r}_2^2 + {r_2}^2\dot{\theta}^2 - 2R\dot{\theta}\dot{r}_2\cos(\theta + 120°) + 2Rr_2\dot{\theta}^2\sin(\theta + 120°)$$

$$v_3^2 = R^2\dot{\theta}^2 + \dot{r}_3^2 + {r_3}^2\dot{\theta}^2 - 2R\dot{\theta}\dot{r}_3\cos(\theta - 120°) + 2Rr_3\dot{\theta}^2\sin(\theta - 120°).$$

In the kinetic energy expression above, it is implicitly assumed that the friction force between the disk and the ground prevents the disk from slipping. The potential energy of the system is expressed as

$$V = mg[r_1\sin\theta + r_2\sin(\theta + 120°) + r_3\sin(\theta - 120°)]. \tag{12}$$

Using the expressions for kinetic and potential energies, Lagrange's equation ([12]) for the generalized coordinate θ can be written as

$$\begin{aligned} &I_{ds}\ddot{\theta} + 3mR^2\ddot{\theta} + m\ddot{\theta}(r_1^2 + r_2^2 + r_3^2) + 2m\dot{\theta}(r_1\dot{r}_1 + r_2\dot{r}_2 + r_3\dot{r}_3) \\ &\quad - mR(\ddot{r}_1\cos\theta + \ddot{r}_2\cos(\theta + 120°) + \ddot{r}_3\cos(\theta - 120°)) \\ &\quad + 2mR\ddot{\theta}(r_1\sin\theta + r_2\sin(\theta + 120°) \\ &\quad + r_3\sin(\theta - 120°)) \\ &\quad + 2mR\dot{\theta}(\dot{r}_1\sin\theta + \dot{r}_2\sin(\theta + 120°) \\ &\quad + \dot{r}_3\sin(\theta - 120°)) + mR\dot{\theta}^2(r_1\cos\theta \\ &\quad + r_2\cos(\theta + 120°) + r_3\cos(\theta - 120°)) + mg(r_1\cos\theta \\ &\quad + r_2\cos(\theta + 120°) + r_3\cos(\theta - 120°)) = 0. \end{aligned} \tag{13}$$

The approximate and optimal solutions in Section 3 indicate that constant angular acceleration of the disk can be generated by periodic trajectories of the unbalance masses. This motivates us to seek periodic solutions from the dynamic analysis as well. We assume r_1, r_2, and r_3 to be periodic functions of the form

$$r_1 = Rf_1(\theta), \quad r_2 = Rf_2(\theta), \quad r_3 = Rf_3(\theta),$$
$$0 \leqslant f_1(\theta), f_2(\theta), f_3(\theta) \leqslant 1 \tag{14}$$

where f_1, f_2, f_3 are dimensionless variables. In the sequel we will establish that there exists a class of periodic trajectories for r_1, r_2, and r_3, that impart constant angular acceleration to the disk. From an implementation point of view, radial forces provided by suitable actuators will guarantee that the unbalance masses track their periodic trajectories. Since our main objective is to investigate the effect of the periodic trajectories on the overall motion of the disk, we do not pursue further analysis of the radial forces. One can easily determine these radial forces or control inputs from the right-hand sides of Lagrange's equations for the generalized coordinates r_1, r_2, and r_3. To continue with our analysis, we use Eq. (14) to rewrite Eq. (13) in the form

$$a(\theta)\ddot{\theta} + b(\theta)\dot{\theta}^2 + c(\theta) = 0$$

$$a(\theta)=I_{ds}+mR^2[3+f_1^2+f_2^2+f_3^2+2(f_1\sin\theta+f_2\sin(\theta+120°)+f_3\sin(\theta-120°))-(f_1'\cos\theta+f_2'\cos(\theta+120°)+f_3'\cos(\theta-120°))]$$

$$b(\theta)=mR^2[2(f_1f_1'+f_2f_2'+f_3f_3')-(f_1''\cos\theta+f_2''\cos(\theta+120°+f_3''\cos(\theta-120°))+2(f_1'\sin\theta+f_2'\sin(\theta+120°)+f_3'\sin(\theta-120°))+(f_1\cos\theta+f_2\cos(\theta+120°)+f_3\cos(\theta-120°))]$$

$$c(\theta)=mgR(f_1\cos\theta+f_2\cos(\theta+120°)+f_3\cos(\theta-120°)) \tag{15}$$

For a constant acceleration maneuver, $\ddot{\theta}=\lambda_1$, we will have $\dot{\theta}=\lambda_1 t+\lambda_2$, where λ_1 and λ_2 are constants. We can then argue that $b(\theta)=0$, or else $\ddot{\theta}$ will increase with time according to the relation

$$\ddot{\theta}=-\frac{b}{a}(\lambda_1 t+\lambda_2)^2-\frac{c}{a}. \tag{16}$$

From Eqs. (15) one can readily show that $b(\theta)=0$ implies

$$(f_1^2+f_2^2+f_3^2)+(f_1\sin\theta+f_2\sin(\theta+120°)+f_3\sin(\theta-120°))-(f_1'\cos\theta+f_2'\cos(\theta+120°)+f_3'\cos(\theta-120°))=\alpha_0 \tag{17}$$

where α_0 is a constant of integration. Apart from $b(\theta)=0$, we also need (c/a) to be constant, or both c and a to be constant, for a constant acceleration maneuver.

4.2 Uniform Acceleration With Constant Potential Energy

Consider the case where both c and a are constant. Rewriting $a(\theta)$ in Eq. (15) as

$$a(\theta)=I_{ds}+mR^2[3+\alpha_0+f_1\sin\theta+f_2\sin(\theta+120°)+f_3\sin(\theta-120°)] \tag{18}$$

and from the expression of $c(\theta)$ in Eq. (15), we get the identities

$$f_1\cos\theta+f_2\cos(\theta+120°)+f_3\cos(\theta-120°)=\alpha_1 \tag{19}$$

$$f_1\sin\theta+f_2\sin(\theta+120°)+f_3\sin(\theta-120°)=\alpha_2 \tag{20}$$

where α_1 and α_2 are constants. From Eqs. (12), (14), and (20) it is established that constant values of c and a lead to constant acceleration maneuvers with potential energy conservation. To proceed further, we differentiate Eq. (19) and substitute Eq. (20) to get

$$f_1'\cos\theta+f_2'\cos(\theta+120°)+f_3'\cos(\theta-120°)=\alpha_2.$$

Substituting this result and Eq. (20) into Eq. (17), we get

$$(f_1^2+f_2^2+f_3^2)=\alpha_0. \tag{21}$$

Using Eqs. (19), (20), and (21), the following expressions for the dimensionless variables f_1, f_2, and f_3 can be obtained:

$$f_1=X\cos(\theta-\phi)+Y \quad X\triangleq(2/3)\{\alpha_1^2+\alpha_2^2\}^{1/2}$$

$$f_2=X\cos(\theta-\phi+120°)+Y \quad Y\triangleq(1/3)\{3\alpha_0-2(\alpha_1^2+\alpha_2^2)\}^{1/2} \tag{22}$$

$$f_3=X\cos(\theta-\phi-120°)+Y \quad \phi\triangleq\arctan(\alpha_2/\alpha_1)$$

where X, Y, ϕ, are constants. From the expressions of X and Y it is clear that both were chosen to be positive square roots. This does not cause any loss of generality and is explained as follows. Irrespective of the sign of X, $X\cos(\theta-\phi)$ takes both positive and negative values. To satisfy the constraint $f_1\geqslant 0$ in Eq. (14), Y must therefore be positive. A change in sign of X is equivalent to a phase shift in ϕ by 180 deg. Therefore X is arbitrarily chosen to be positive. The above analysis confirms that f_1,f_2,f_3, and accordingly r_1,r_2,r_3, have identical trajectories, shifted in phase.

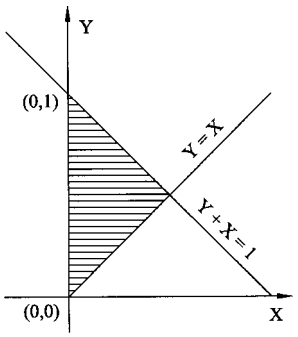

Fig. 6 Shaded region indicates feasible parameter values for the solution in Section 4.2

The trajectories in Eq. (22) are limacons, similar to those obtained in Section 3.2. This is surprising since the analysis in Section 3.2 was carried out with a static model whereas the complete dynamic model was employed in this section. The main difference between the two trajectories are in the number of defining parameters. The limacons in Section 3.2 are defined by two parameters, C_2 and K, as seen from Eq. (11). In this section the limacons are defined by three parameters, namely X, Y, and ϕ. The advantage of having three independent parameters is that any initial configuration of the three masses can determine the trajectories and the corresponding acceleration. From Eqs. (15), (16), (19), and (20), the disk acceleration can be expressed as

$$\ddot{\theta}=-\left[\frac{mgR\alpha_1}{I_{ds}+mR^2(3+\alpha_0+\alpha_2)}\right] \tag{23}$$

where $\alpha_0,\alpha_1,\alpha_2$ can be expressed in terms of trajectory parameters X, Y, ϕ as follows:

$$\alpha_0\triangleq 1.5X^2+3.0Y^2, \quad \alpha_1\triangleq 1.5X\cos\phi, \quad \alpha_2\triangleq 1.5X\sin\phi. \tag{24}$$

While arbitrary initial conditions can uniquely define a trajectory, not all trajectories will satisfy the physical constraints of Eq. (14). For feasibility, X,Y must lie in the shaded region, shown in Fig. 6. This is quite similar to the constraint imposed on the parameters of the trajectory in Section 3.2, shown in Fig. 4.

Although initial values of f_1, f_2, f_3, and θ uniquely define the trajectory parameterized by $\alpha_0,\alpha_1,\alpha_2$, or X,Y,ϕ, and uniquely define the acceleration of the disk $\ddot{\theta}$, the converse is not true: A given acceleration of the disk can be generated through various trajectories.

4.3 Effect of Variation of Path Parameters

Effect of Varying Phase Angle. Using Eqs. (23) and (24), the disk acceleration can be written as

$$\ddot{\theta}=-\left[\frac{1.5mgRX\cos\phi}{I_{ds}+1.5mR^2(2+X\sin\phi+X^2+2Y^2)}\right]=\frac{\beta\cos\phi}{\mu+\sin\phi} \tag{25}$$

where β and μ are constants, given by the relations

$$\beta\triangleq-\frac{g}{R}, \quad \mu\triangleq\frac{I_{ds}+1.5mR^2(2+X^2+2Y^2)}{1.5mR^2X}. \tag{26}$$

From the expression of μ, and feasible values of X in Fig. 6, it can be shown that the denominator in Eq. (25) is always positive. The

sign of $\ddot{\theta}$ therefore depends on the sign of $\cos\phi$, or $X\cos\phi$ since X is always positive. Specifically, $\ddot{\theta}$ is positive if $X\cos\phi$ is negative and vice versa. With Eqs. (19) and (24) it can be established that the z-coordinate of the center of mass, relative to the center of the disk, is located at

$$z_{cm}=\frac{R}{3}[f_1\cos(\pi+\theta)+f_2\cos(\pi+\theta+120°)+f_3\cos(\pi+\theta-120°)]=-\frac{R}{3}\alpha_1=-\frac{R}{2}X\cos\phi.$$

The above equation implies that the magnitude and direction of acceleration depends primarily on the z-coordinate of the center of mass, relative to the center of disk.

The rolling disk can acquire a range of acceleration by varying phase angle ϕ. From Eq. (25), the maximum and minimum values of the acceleration can be shown to be

$$\ddot{\theta}=\begin{cases}\ddot{\theta}_{\max} & \text{if } \phi=\pi+\arcsin(1/\mu)\\ \ddot{\theta}_{\min} & \text{if } \phi=-\arcsin(1/\mu).\end{cases} \tag{27}$$

Of course, motion with zero acceleration or constant velocity requires $\phi=\pm\pi/2$. From an implementation point of view, the rolling disk can change ϕ during its motion by suppressing the motion of the masses for an appropriate interval of time.

*Effect of Varying Parameters **X** and **Y**.* Each point in the shaded region of Fig. 6 corresponds to a certain trajectory of the disk; each of these trajectories has a certain acceleration. Clearly, a variation in X and Y is expected to provide a range of accelerations. By treating ϕ as constant, we partially differentiate $\ddot{\theta}$ in Eq. (25) with respect to X and Y. Equating these expressions to zero, the maximum $\ddot{\theta}$ is observed to occur at the following coordinate:

$$X=\sqrt{2(1+I_{ds}/3mR^2)},\quad Y=0$$

independent of the value of ϕ. Unfortunately, this coordinate lies outside the shaded region in Fig. 6. Since the above coordinate is the only location where $\ddot{\theta}$ is an extremum, we conclude that the maximum feasible $\ddot{\theta}$ occurs at a point, or a set of points on the boundary of the shaded region. Through numerical simulation we determined the maximum to occur at $(X,Y)=(0.5,0.5)$. Combining this result with the result in Eq. (27), we conclude that the trajectories that produce maximum and minimum acceleration are

$$\ddot{\theta}=\begin{cases}\ddot{\theta}_{\max} & \text{if } f_1=-0.5\cos[\theta-\arcsin(1/\bar{\mu})]+0.5\\ \ddot{\theta}_{\min} & \text{if } f_1=0.5\cos[\theta+\arcsin(1/\bar{\mu})]+0.5\end{cases},\qquad \bar{\mu}\triangleq\frac{I_{ds}+4.125mR^2}{0.75mR^2}$$

where $\bar{\mu}$, obtained from Eq. (26), is the value of μ evaluated at $X=Y=0.5$. Instead of numerical simulation, the above result for maximum acceleration can also be obtained through constrained optimization.

5 Dynamic Model: Variable Potential Energy Maneuvers

5.1 Uniform Acceleration With Variable Potential Energy It was shown in Section 4.1 that constant acceleration maneuvers require (c/a) to be constant. The analysis in Sections 4.2 and 4.3 was carried out assuming both c and a as constants, which leads to conservation of potential energy. In an effort to generalize the results, we investigate the case of varying potential energy in this section. We treat c and a as variables whose ratio is constant. We begin our analysis with the expression for the potential energy. Using Eqs. (12) and (14), V can be expressed as

$$V=mgR[f_1\sin\theta+f_2\sin(\theta+120°)+f_3\sin(\theta-120°)].$$

It can be shown that V satisfies $-mgR\leqslant V\leqslant mgR$. In compliance with these limits and without loss of generality, we consider a sinusoidal variation in V, given by the relation

$$V=mgR[A_1+B_1\sin(\theta-\psi)]$$

where A_1, B_1, and ψ are constants. By comparing the above two equations, we can write

$$f_1\sin\theta+f_2\sin(\theta+120°)+f_3\sin(\theta-120°)=A_1+B_1\sin(\theta-\psi). \tag{28}$$

We have $b(\theta)=0$ for constant acceleration maneuvers. Using the expressions for $c(\theta)$ and $a(\theta)$ in Eqs. (15) and (18), the equation of motion in Eq. (16) reduces to the form

$$\ddot{\theta}\{I_{ds}+mR^2[3+\alpha_0+f_1\sin\theta+f_2\sin(\theta+120°)+f_3\sin(\theta-120°)]\}=-mgR[f_1\cos\theta+f_2\cos(\theta+120°)+f_3\cos(\theta-120°)]. \tag{29}$$

Substituting Eq. (28) in Eq. (29), we get

$$\ddot{\theta}\{K_1+K_2[A_1+B_1\sin(\theta-\psi)]\}=f_1\cos\theta+f_2\cos(\theta+120°)+f_3\cos(\theta-120°)$$

$$K_1\triangleq-\frac{I_{ds}+mR^2(3+\alpha_0)}{mgR},\quad K_2\triangleq-\frac{R}{g}. \tag{30}$$

For a constant magnitude of acceleration, $\ddot{\theta}=G$, we can then write

$$f_1\cos\theta+f_2\cos(\theta+120°)+f_3\cos(\theta-120°)=A_2+B_2\sin(\theta-\psi)$$

$$A_2=G(K_1+A_1K_2),\quad B_2=GB_1K_2. \tag{31}$$

Using Eqs. (28) and (31), Eq. (17) can now be written as

$$f_1^2+f_2^2+f_3^2=\alpha_0+B_2\cos(\theta-\psi) \tag{32}$$

where it is obvious that $\alpha_0\geqslant|B_2|$. From Eqs. (28), (31), and (32), f_1, f_2, and f_3 can be solved as follows:

$$f_1=\frac{2}{3}P_1\pm\frac{1}{3}\sqrt{3(\alpha_0+B_2\cos(\theta-\psi))-2S}$$

$$f_2=\frac{2}{3}P_2\pm\frac{1}{3}\sqrt{3(\alpha_0+B_2\cos(\theta-\psi))-2S}$$

$$f_3=\frac{2}{3}P_3\pm\frac{1}{3}\sqrt{3(\alpha_0+B_2\cos(\theta-\psi))-2S}$$

where S and P_j, $j=1,2,3$, are defined as

$$S\triangleq[A_1+B_1\sin(\theta-\psi)]^2+[A_2+B_2\sin(\theta-\psi)]^2$$

$$P_j\triangleq[A_1+B_1\sin(\theta-\psi)]\sin[\theta+(j-1)120°]+[A_2+B_2\sin(\theta-\psi)]\cos[\theta+(j-1)120°].$$

It can be verified from the above equation that $(P_1+P_2+P_3)=0$. Using this result the common term in the expressions of f_1, f_2, f_3 can be shown to be $(f_1+f_2+f_3)/3$. It immediately follows that the nontrivial solution for f_1, f_2, f_3 is

$$f_1=\frac{2}{3}P_1+\frac{1}{3}\sqrt{3(\alpha_0+B_2\cos(\theta-\psi))-2S}$$

$$f_2=\frac{2}{3}P_2+\frac{1}{3}\sqrt{3(\alpha_0+B_2\cos(\theta-\psi))-2S} \tag{33}$$

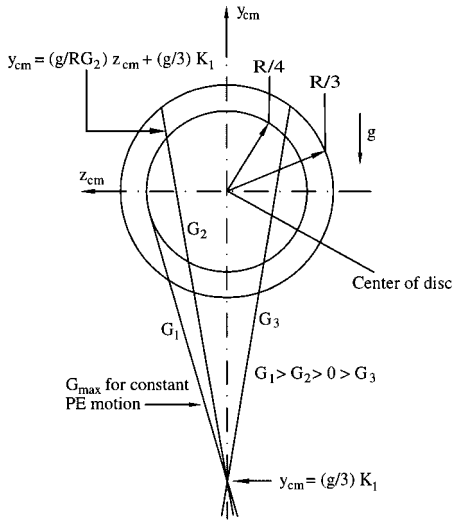

Fig. 7 A geometric interpretation of the motion of the center of mass

$$f_3 = \frac{2}{3} P_3 + \frac{1}{3}\sqrt{3(\alpha_0 + B_2\cos(\theta - \psi)) - 2S}.$$

From Eqs. (22) and (33) it can be seen that trajectories conserving potential energy are identical for the three masses except for the 120 deg phase shift; this is not true for variable potential energy. Also, the trajectories in Eq. (22) are limacons, described by three parameters. The trajectories in Eq. (33), which are not limacons, require five parameters for their description. These parameters are A_1, B_1, G, ψ, and α_0.

5.2 Motion of the Center of Mass. The coordinates of the center-of-mass of the system can be written as

$$z_{cm} = -\frac{R}{3}[f_1\cos\theta + f_2\cos(\theta + 120°) + f_3\cos(\theta - 120°)]$$

$$y_{cm} = \frac{R}{3}[f_1\sin\theta + f_2\sin(\theta + 120°) + f_3\sin(\theta - 120°)].$$

Using these relations, Eq. (29) can be written as

$$\ddot{\theta}\{I_{ds} + mR^2(3 + \alpha_0) + 3mRy_{cm}\} = 3mgz_{cm}.$$

For a constant acceleration $\ddot{\theta} = G$, this reduces to

$$y_{cm} = \frac{g}{RG} z_{cm} + \frac{g}{3} K_1 \tag{34}$$

where K_1 was defined in Eq. (30). Also note that the distance of the center-of-mass from the disk center is constrained by the relation

$$y_{cm}^2 + z_{cm}^2 \leqslant (R/3)^2. \tag{35}$$

The proof of the above relation is simple and left to the reader. Some observations on the motion of the disk, evident from Eqs. (34) and (35), are now discussed with the help of Fig. 7.

1. Straight lines with different slopes represent different magnitudes (G) of acceleration. A line with a positive slope represents acceleration and a line with a negative slope represents deceleration. A horizontal line in Fig. 7 represents constant velocity motion.

2. A feasible trajectory of the disk requires the straight line in Eq. (34) to pass through the circular region defined by Eq. (35). However, this is not sufficient to guarantee that the physical constraints, $0 \leqslant f_1, f_2, f_3 \leqslant 1$, will be met. This is true for the same reason the center-of-mass may remain bounded when individual mass positions become unbounded.

3. Since α_0 is positive, which can be shown from Eq. (32), the intercept of the straight line in Eq. (34) on the y-axis is negative, and outside the circle defined by Eq. (35). This confirms that the range of acceleration of the disk, determined by the slope of the line, is finite.

4. A feasible trajectory is described by sinusoidal variation in both center-of-mass coordinates, y_{cm} and z_{cm}. This, evident from Eqs. (28) and (31), translates to the center-of-mass position oscillating along a straight line, while remaining confined to the circle of radius $R/3$ in Fig. 7. In contrast, when the potential energy is conserved, y_{cm} remains stationary. This implies that the center-of-mass position will remain stationary.

5. From the range of X in Fig. 6, namely $X \leqslant 0.5R$, and expressions for α_1, α_2, in Eq. (24), we have $-0.75 \leqslant \alpha_1, \alpha_2 \leqslant 0.75$. Using Eqs. (19) and (20) we can therefore show that y_{cm}, z_{cm} are individually constrained to lie between $\pm R/4$. This indicates that for constant potential energy maneuvers the straight line in Eq. (34) must intersect, or be tangential to, a smaller circle of radius $R/4$. This indicates that the variable potential energy case holds the promise for higher acceleration.

6 Tracking an Acceleration Profile

6.1 An Optimal Approach to Tracking Acceleration. In this section we present an optimal method for tracking an acceleration profile. We compute discrete changes in acceleration over small intervals of time and seek to determine changes in trajectory parameters that minimize the cost functional

$$J = \int_0^{2\pi} (\Delta f_1)^2\, d\theta.$$

The basic trajectories can be chosen to be the limacons in Eq. (22) or the more complex forms in Eq. (33). For simplicity, we choose the limacons which are described by fewer parameters. Though the limacons conserve potential energy, we do not expect the potential energy to remain conserved as we track an acceleration profile. This is true since the limacon parameters will continually change during acceleration tracking. While a different cost function could have been chosen, the cost function above promises to minimize the overall change in the shape of the trajectory, which is identical for all three masses. On differentiating f_1 in Eq. (22), we obtain

$$\Delta f_1 = \cos(\theta - \phi)\Delta X + X\sin(\theta - \phi)\Delta\phi + \Delta Y. \tag{36}$$

Substituting Eq. (36) into the expression of J, we get

$$J = \pi\Delta X^2 + \pi(X\Delta\phi)^2 + 2\pi\Delta Y^2.$$

We now rewrite Eq. (23) as

$$\ddot{\theta} = \frac{\beta\alpha_1}{\nu + \alpha_2 + \alpha_0}, \quad \nu \triangleq 3 + \frac{I_{ds}}{mR^2}. \tag{37}$$

A change in $\ddot{\theta}$ can therefore be expressed in terms of changes in path parameters, as follows:

$$\Delta\ddot{\theta} = \left(\frac{\ddot{\theta}}{\alpha_1}\right)\Delta\alpha_1 - \left(\frac{\ddot{\theta}^2}{\beta\alpha_1}\right)\Delta\alpha_2 - \left(\frac{\ddot{\theta}^2}{\beta\alpha_1}\right)\Delta\alpha_0. \tag{38}$$

Substituting Eqs. (24) and (38) into the expression of J, we get

$$J = \frac{4\pi}{9}(\Delta\alpha_1{}^2 + \Delta\alpha_2{}^2) + \frac{\pi}{2}\frac{\{(3\beta\ddot{\theta} - 4\alpha_1\ddot{\theta}^2)\Delta\alpha_1 - (3 + 4\alpha_2)\ddot{\theta}^2\Delta\alpha_2 - 3\beta\Delta\ddot{\theta}\alpha_1\}^2}{[3\alpha_0 - 2(\alpha_1^2 + \alpha_2^2)]}.$$

By computing the partial derivatives of J with respect to α_1, α_2, and equating them to zero, we obtain optimal change in path parameters $\Delta\alpha_1, \Delta\alpha_2$,

$$\Delta\alpha_1 = \frac{9\gamma_1\gamma_2\gamma_4}{8\pi + 9\gamma_1(\gamma_2^2+\gamma_3^2)}, \quad \Delta\alpha_2 = -\frac{9\gamma_1\gamma_3\gamma_4}{8\pi + 9\gamma_1(\gamma_2^2+\gamma_3^2)}, \tag{39}$$

where γ_1, γ_2, γ_3, and γ_4 are defined as

$$\gamma_1 = \frac{\pi}{3\alpha_0 - 2(\alpha_1^2+\alpha_2^2)} \quad \gamma_3 = \left(1 + \frac{4}{3}\alpha_2\right)$$

$$\gamma_2 = \left(\frac{\beta}{\ddot{\theta}} - \frac{4}{3}\alpha_1\right) \quad \gamma_4 = \frac{\beta\Delta\ddot{\theta}\alpha_1}{\ddot{\theta}^2}.$$

Though it may seem that $\Delta\alpha_1$ grows unbounded when $\ddot{\theta}$ is zero, this is not the case. By integrating the expression for $\Delta\alpha_1$, we can show that the following relation is true:

$$\frac{1}{\alpha_1} = \sigma\left[\frac{\beta^2}{\ddot{\theta}^2} + \left(1 - \frac{8}{3}\nu\right)\right]^{1/2} - \frac{4\beta}{(3-8\nu)\ddot{\theta}}$$

where σ is a constant of integration, and β and ν are constants that have been defined in Eqs. (26) and (37), respectively. Clearly, as $\ddot{\theta}$ tends to zero, α_1 tends to zero and $\Delta\alpha_1$ remains finite.

The optimal change in parameter α_0, namely $\Delta\alpha_0$, can now be computed from Eqs. (38) and (39). The changes in parameters α_1, α_2, α_0, can be translated into equivalent changes in X, Y, ϕ, using the following equation:

$$\begin{pmatrix}\Delta X\\ \Delta Y\\ \Delta\phi\end{pmatrix} = \frac{2}{3}\begin{pmatrix}\cos\phi & 0 & X\sin\phi\\ \sin\phi & 0 & X\cos\phi\\ 2X & 4Y & 0\end{pmatrix}^{-1}\begin{pmatrix}\Delta\alpha_1\\ \Delta\alpha_2\\ \Delta\alpha_0\end{pmatrix} \tag{40}$$

which was derived from Eq. (22). The matrix in Eq. (40) becomes singular when either X or Y is zero. This should not be of concern since $X=0$ and $Y=0$ are limiting values for a feasible trajectory, as evident from Fig. 6. The matrix is also singular when $X=1$ and $\phi=\pi/4$. This point clearly lies outside the range of feasible parameter values and should also be of no concern. After computing the changes in X, Y, ϕ, the change in the trajectory of m_1 can be computed from Eq. (36). The changes in trajectories of m_2 and m_3 can be computed similarly.

6.2 Simulation Results. In this section we present simulation results of the disk tracking a sinusoidal acceleration profile. The initial angle of the disk in radians, and position of the three masses in dimensionless variables are given as

$$\theta(0)=0.8, \quad f_1[\theta(0)]=0.7, \quad f_2[\theta(0)]=0.4, \quad f_3[\theta(0)]=0.3.$$

The values of $\alpha_0, \alpha_1, \alpha_2$ are first computed using Eqs. (19), (20), and (21). Subsequently, the initial acceleration of the disk is obtained using Eq. (23) as $\ddot{\theta}(0) = -3.28\ \text{rad/s}^2$. For our simulation, we choose the acceleration profile

$$\ddot{\theta} = -2.0 + 8.5\sin(0.5t - \zeta) \tag{41}$$

with the proper choice of ζ that satisfies the initial condition $\ddot{\theta}(0) = -3.28\ \text{rad/s}^2$. We also choose $\beta \triangleq -(g/R) = -100$ in SI units, and $\nu \triangleq 3 + (I_{ds}/mR^2) = 4.5$. The simulation is carried out over 60 seconds using a time-step of 0.001 second. At each time-step the trajectory parameters X, Y, are verified to lie in the shaded region of Fig. 6. This guarantees that physical constraints are not violated.

The simulation results are shown in Figs. 8 and 9. Figure 8 is a plot of trajectory parameters X, Y, and ϕ for the acceleration profile in Eq. (41). As expected, the trajectory of ϕ has the same frequency as that of the acceleration profile. The trajectory of X is more interesting and has two peaks in every cycle of acceleration.

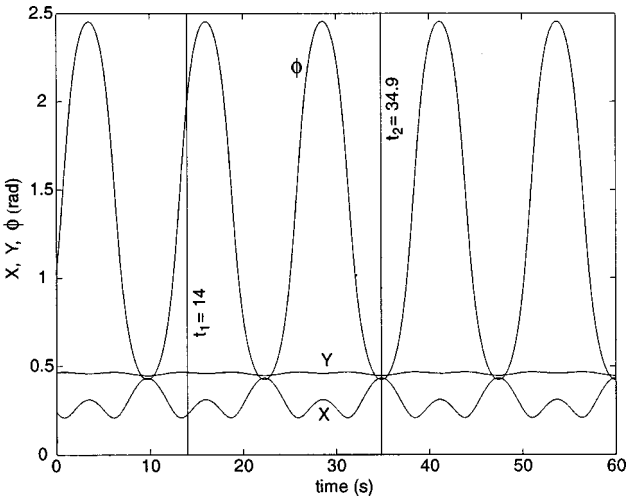

Fig. 8 Variation of trajectory parameters during a sinusoidal variation of acceleration

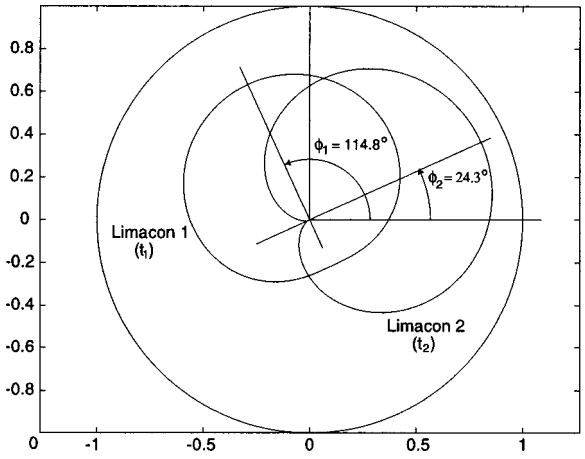

Fig. 9 Normalized trajectories of the unbalance masses at two specific instants of time

Since X represents the radial distance of the center-of-mass, it assumes maximal values for both the maximum and minimum acceleration. However, since magnitudes of the maximum and minimum acceleration are different (6.5 rad/s^2 and -10.5 rad/s^2, respectively), the peaks differ in magnitude. The shape of the limacon in Eq. (22), which changes as a function of the trajectory parameters, is shown in Fig. 9 for two specific instants of time, $t_1 = 14.0$ seconds and $t_2 = 34.9$ seconds. At these instants of time, the limacon is seen to have the following parametric representations:

$$f_1(\theta) = \begin{cases} 0.229\cos(\theta - 114.8°) + 0.467 & \text{for } t = t_1 \\ 0.435\cos(\theta - 24.3°) + 0.448 & \text{for } t = t_2. \end{cases}$$

7 Conclusion

This paper investigates a self-propulsion mechanism comprised of three unbalance masses for a vertically upright rolling disk constrained to move along a straight line path. It is shown that trajectories of the unbalance masses can be designed to propel the disk with a wide range of accelerations. It is also shown that the disk can track an acceleration profile while minimizing an appropriate cost function. In the preliminary analysis, where a static model was used, uniform acceleration maneuvers assumed conser-

vation of potential energy. The potential energy plays an important role throughout the analysis, and hence both constant and variable potential energy cases were considered with the dynamic model. Under conservation of potential energy, the dynamic model results in trajectories similar to those obtained from the static model; the results obtained from the dynamic model are, however, more general. With both models, the trajectories of the unbalance masses are identical limacons with phase shifts of 120 deg. This is not true for the case of variable potential energy. In this most general case, the center-of-mass oscillates along a straight line while the disk undergoes constant acceleration. For all the cases considered, it was observed that a prescribed acceleration could be achieved using multiple trajectories or multiple initial conditions; a set of initial conditions, however, uniquely defines the trajectories and the acceleration. Some simulation results were also presented in this paper. For a prescribed sinusoidal acceleration profile, minimum variation in trajectory parameters were simulated.

Acknowledgment

The authors gratefully acknowledge the support provided by National Science Foundation, NSF Grant No. CMS-9800343, in carrying out this research.

References

[1] Brown, H. B., and Xu, Y., 1997, ''A Single-Wheel Gyroscopically Stabilized Robot,'' IEEE Robotics and Automation Magazine, **4**, No. 3, pp. 39–44.
[2] Koshiyama, A., and Yamafuji, K., 1993, ''Design and Control of All-Direction Steering Type Mobile Robot,'' Int. J. Robot. Res., **12**, No. 5, pp. 411–419.
[3] Halme, A., Schonberg, T., and Wang, Y., 1996, ''Motion Control of a Spherical Mobile Robot,'' *Proc. AMC'96-MIE*.
[4] Bicchi, A., Balluchi, A., Prattichizzo, D., and Gorelli, A., 1997, ''Introducing the Sphericle: An Experimental Testbed for Research and Teaching in Nonholonomy,'' *Proc. IEEE Int. Conference on Robotics and Automation*, pp. 2620–2625.
[5] Mukherjee, R., and Minor, M., 1999, ''A Simple Motion Planner for a Spherical Mobile Robot,'' IEEE/ASME Int. Conference on Advanced Intelligent Mechatronics, Atlanta, GA.
[6] Ehlers, G. W., Yavin, Y., and Frangos, C., 1996, ''On the Motion of a Disk Rolling on a Horizontal Plane: Path Controllability and Feedback Control,'' Comput. Methods Appl. Mech. Eng., **137**, pp. 345–356.
[7] Yavin, Y., 1997, ''Inclination Control of the Motion of a Rolling Disk by Using a Rotor,'' Comput. Methods Appl. Mech. Eng., **146**, pp. 253–263.
[8] Yavin, Y., 1999, ''Stabilization and Motion Control of the Motion of a Rolling Disk by Using Two Rotors Fixed Along Its Axis,'' Comput. Methods Appl. Mech. Eng., **169**, pp. 107–122.
[9] Getz, N., 1995, ''Internal Equilibrium Control of a Bicycle,'' 34th IEEE Conference on Decision and Control, New Orleans, LA.
[10] Rui, C., and McClamroch, N. H., 1995, ''Stabilization and Asymptotic Path Tracking of a Rolling Disk,'' 34th IEEE Conference on Decision and Control, New Orleans, LA.
[11] Kirk, D. E., 1970, *Optimal Control Theory: An Introduction*, Prentic-Hall, Englewood Cliffs, NJ.
[12] Greenwood, D. T., 1988, *Principles of Dynamics*, Prentice-Hall, Englewood Cliffs, NJ.